
Article:
The IMBIE Team, , Shepherd, A orcid.org/0000-0002-4914-1299, Ivins, E et al. (78 more authors) (2018) Mass balance of the Antarctic Ice Sheet from 1992 to 2017. Nature, 558. pp. 219-222. ISSN 0028-0836

https://doi.org/10.1038/s41586-018-0179-y

Mass balance of the Antarctic ice sheet from 1992 to 2017

The IMBIE team

Andrew Shepherd[1,*], Erik Ivins[2], Eric Rignot[3], Ben Smith[4], Michiel van den Broeke[5], Isabella Velicogna[3], Pippa Whitehouse[6], Kate Briggs[1], Ian Joughin[4], Gerhard Krinner[7], Sophie Nowicki[8], Tony Payne[9], Ted Scambos[10], Nicole Schlegel[11], Geruo A[3], Cécile Agosta[12], Andreas Ahlstrøm[13], Greg Babonis[14], Valentina Barletta[15], Alejandro Blazquez[16], Jennifer Bonin[17], Beata Csatho[18], Richard Cullather[19], Denis Felikson[20], Xavier Fettweis[12], Rene Forsberg[15], Hubert Gallee[21], Alex Gardner[11], Lin Gilbert[22], Andreas Groh[23], Brian Gunter[24], Edward Hanna[25], Christopher Harig[26], Veit Helm[27], Alexander Horvath[28], Martin Horwath[23], Shfaqat Khan[15], Kristian K. Kjeldsen[29,13], Hannes Konrad[1], Peter Langen[30], Benoit Lecavalier[31], Bryant Loomis[8], Scott Luthcke[8], Malcolm McMillan[1], Daniele Melini[32], Sebastian Mernild[33,34,35], Yara Mohajerani[3], Philip Moore[36], Jeremie Mouginot[3,21], Gorka Moyano[37], Alan Muir[22], Thomas Nagler[38], Grace Nield[6], Johan Nilsson[11], Brice Noel[5], Ines Otosaka[1], Mark E. Pattle[37], W. Richard Peltier[39], Nadege Pie[20], Roelof Rietbroek[40], Helmut Rott[38], Louise Sandberg-Sørensen[15], Ingo Sasgen[27], Himanshu Save[20], Ernst Schrama[41], Ludwig Schröder[23], Ki-Weon Seo[42], Sebastian Simonsen[15], Tom Slater[1], Giorgio Spada[43], Tyler Sutterley[3], Matthieu Talpe[10], Lev Tarasov[31], Willem Jan van de Berg[5], Wouter van der Wal[41], Melchior van Wessem[5], Bramha Dutt Vishwakarma[44], David Wiese[11], Bert Wouters[5]

1. University of Leeds; 2. Jet Propulsion Lab; 3. University of California Irvine; 4. University of Washington; 5. Utrecht University; 6. Durham University; 7. CNRS; 8. NASA GSFC; 9. University of Bristol; 10. University of Colorado; 11. NASA JPL; 12. University of Liège; 13. Geological Survey of Denmark and Greenland; 14. State University of New York at Buffalo; 15. DTU Space; 16. LEGOS; 17. University of South Florida; 18. University at Buffalo; 19. NASA GMAO; 20. University of Texas ; 21. University Grenoble Alpes; 22. University College London; 23. Technische Universitat Dresden; 24. Georgia Institute of Technology; 25. University of Lincoln; 26. University of Arizona; 27. AWI Helmholtz Zentrum; 28. Technical University Munich; 29. Natural History Museum of Denmark; 30.

Danish Meteorological Institute; 31. Memorial University of Newfoundland; 32. INGV; 33. Nansen Environmental and Remote Sensing Center; 34. Western Norway University of Applied Sciences; 35. Universidad de Magallanes; 36. Newcastle University; 37. isardSAT; 38. ENVEO Gmbh; 39. University of Toronto; 40. University of Bonn; 41. Delft University of Technology; 42. Seoul National University; 43. Urbino University; 44. University of Stuttgart

*Corresponding author: Andrew Shepherd a.shepherd@leeds.ac.uk

The Antarctic ice sheet is an important indicator of climate change and driver of sea level rise. Here, we combine satellite observations of its changing volume, flow, and gravitational attraction and surface mass balance modelling, to show that it lost 2720 ± 1390 Gt of ice between 1992 and 2017 - a 7.6 ± 3.9 mm contribution to mean sea level. Ocean-driven melting has caused rates of ice loss from West Antarctica to rise from 53 ± 29 Gt/yr in the 1990s to 159 ± 26 Gt/yr in the 2010s. Ice shelf collapse has driven Antarctic Peninsula ice loss up from 7 ± 13 Gt/yr in the 1990s to 33 ± 16 Gt/yr in the 2010s. We find large variations in and among model estimates of surface mass balance and glacial isostatic adjustment in East Antarctica, and its 25-year mass trend (5 ± 46 Gt/yr) is still the least certain.

The Antarctic ice sheets hold enough water to raise global sea level by 58 metres [1]. They channel ice to the oceans through a network of glaciers and ice streams [2], each with a substantial inland catchment [3]. Fluctuations in the grounded ice sheet mass arise due to differences between net snow accumulation at the surface, meltwater runoff, and ice discharge into the ocean. In recent decades, reductions in the thickness [4] and extent [5] of floating ice shelves have disturbed inland ice flow, triggering retreat [6,7], acceleration [8,9], and drawdown [10,11] of many marine terminating ice streams. A variety of techniques have been developed to measure changes in ice sheet mass, based on satellite observations of their speed [12], volume [13], and gravitational attraction [14] combined with modelled surface mass balance [15] and glacial isostatic adjustment[16]. Since 1989, there have been more than 150 assessments of ice loss from Antarctica based on these approaches [17]. An inter-comparison of 12

such estimates [18], demonstrated that the three principal satellite techniques provide similar results at the continental scale and, when combined, lead to an estimated mass loss of 71 ± 53 Gt of ice per year averaged over the period 1992 to 2011. Here, we extend this assessment to include twice as many studies, doubling the overlap period and extending the record through to 2017.

We collated 24 independently-derived estimates of ice sheet mass balance (Figure 1) determined within the period 1992 to 2017 and based upon the techniques of satellite altimetry (7 estimates), gravimetry (15 estimates) or the input-output method (2 estimates). Altogether, there were 24, 24, and 23 individual estimates of mass change computed within defined geographical limits [19,20] for the East Antarctic, West Antarctic and the Antarctic Peninsula ice sheets, respectively. Rates of ice sheet mass change were compared (see Methods) over common intervals of time [18]. We then averaged rates of ice sheet mass balance based on the same class of satellite observations to produce three technique-dependent time series of mass change in each geographical region (see Methods). Within each class, the annual mass rate uncertainty was computed as the mean uncertainty of the individual contributions. The final, reconciled estimate of ice sheet mass change for each region was computed as the mean of the technique-dependent values available at each epoch (Figure 1). In computing the associated uncertainty, we assumed that the errors for each technique are independent. To estimate the cumulative mass change and its uncertainty (Figure 2), we integrated the reconciled estimates for each ice sheet and weighted the annual uncertainty by $1/\sqrt{n}$, where n is the number of years elapsed relative to the start of each time series. Antarctic ice sheet mass trends and their uncertainties (Table 1) were computed as the linear sum and root sum square of the regional trends and their uncertainties, respectively.

The level of disagreement between individual estimates of ice sheet mass balance increases with the area of each ice sheet region, with average per-epoch standard deviations of 11, 21, and 37 Gt/yr at the Antarctic Peninsula, West Antarctica, and East Antarctica, respectively (Figure 1 and Methods). Among the techniques, gravimetric estimates are the most abundant and also the most closely

aligned, though their spread increases in East Antarctica where glacial isostatic adjustment remains poorly constrained [21] and is least certain when spatially integrated [22-33] due to the region's vast extent. Solutions based on satellite altimetry and the input-output method run for the entire record, roughly twice the duration of the gravimetry time series. Although most (59 %) estimates fall within one standard deviation of the technique-dependent mean, a few (6 %) depart by more than three. At the Antarctic Peninsula, the 25-year average rate of ice sheet mass balance is -20 ± 15 Gt/yr, with a ~15 Gt/yr increase in losses since 2000. The strongest signal and trend has occurred in West Antarctica, where rates of mass loss rise from 53 ± 29 Gt/yr to 159 ± 26 Gt/yr between the first and final 5 years of our survey, with the largest increase occurring during the late 2000's when ice discharge from the Amundsen Sea sector accelerated [34]. Both of these regional losses are driven by reductions in the thickness and extent of floating ice shelves, which has triggering retreat, acceleration, and drawdown of marine terminating glaciers [35]. The least certain result is in East Antarctica, where the average 25-year mass trend is 5 ± 46 Gt/yr. Overall, the Antarctic ice sheet lost 2720 ± 1390 Gt of ice between 1992 and 2017, an average rate of 109 ± 56 Gt/yr.

Knowledge of the ice sheet surface mass balance is an essential component of the input-output method, which subtracts solid ice discharge from net snow accumulation, and also aids interpretation of mass trends derived from satellite altimetry and gravimetry. Snowfall is the major driver of temporal and spatial variability in Antarctic ice sheet surface mass change [36,37]. Although locally important, spatially integrated sublimation and meltwater runoff are typically one to two orders of magnitude smaller, respectively. In the absence of observation-based maps, Antarctic ice sheet surface mass balance is usually taken from atmospheric models, evaluated with in-situ and remotely-sensed observations [15,38-41]. To assess Antarctic surface mass balance, we compared two global reanalysis products (JRA55 and ERA-Interim) and two regional climate models (RACMO2 and MARv3.6)(see Methods). ERA-Interim is usually regarded as the best performing reanalysis product over Antarctica, albeit with a dry bias in the interior and overestimated rain fraction [40,42,43]. Spatially averaged accumulation rates peak at the Antarctic Peninsula, and are ~3 and ~7 times lower in West

and East Antarctica, respectively (Extended Data Figure 2 and Extended Data Figure 3). Compared to the all-model average surface mass balance of 1994 Gt/yr, the regional climate models have 4.7% higher and the reanalyses 7% lower values. These differences can be attributed to the higher resolution of the regional models, which resolve the steep coastal precipitation gradients in greater detail, and also their improved representation of polar processes. The temporal variability of all products is similar, and they all agree on the absence of an ice sheet wide trend in surface mass balance over the period 1979 to 2017, implying that recent Antarctic ice sheet mass loss is dominated by increased solid ice discharge into the ocean.

Gravimetric estimates of mass change are strongly influenced by the method used to correct for glacial isostatic adjustment (GIA)[16]. In this study, six different GIA models were used for this purpose [22,25,27,31,32,44]. We also assessed nine continent-wide forward-model and two regional model simulations to better understand uncertainties in the GIA signal itself, and we reprocessed the gravimetry estimates of mass balance using just the W12a [27] and IJ05_R2 [32] GIA models for comparison with earlier work[18] (see Methods). The net gravitational effect of GIA across Antarctica is positive, and the mean and standard deviation of the continent-wide GIA models (54 ± 18 Gt/yr) is very close to that of W12a (56 ± 27 Gt/yr) and IJ05_R2 (55 ± 13 Gt/yr). The narrow spread likely reflects the difficulty of quantifying the timing and extent of past ice sheet change, and the absence of lateral variations in Earth rheology within some models [45]. In areas where GIA is a significant component of the regional mass change, such as the Amundsen, Ross and Filchner-Ronne sectors of West Antarctica (see Extended Data Figure 4), models predict the greatest uplift rates (5 to 7 mm/yr on average) but also the greatest variability (e.g. standard deviation > 10 mm/yr in the Amundsen sector). Away from areas with large GIA signals there is low variance among the models and broad agreement with GPS observations [46]. Nevertheless, most models considered here do not account for ice sheet change during the last few millennia, because it is poorly known. Inaccurate treatment of low degree harmonics associated with the global GIA signal can also bias gravimetric mass balance

127 calculations [47]. If the GIA signal includes a transient component associated with recent ice sheet
128 change this will bias mass trend estimates and should be accounted for in future work.

129 Improvements in ice sheet mass balance assessments are still possible. Airborne snow radar [48,49] is a
130 powerful tool for evaluating surface mass balance and firn compaction models over large spatial
131 (1000's of km) and temporal (centennial) scales, in addition to the ice cores that have been
132 traditionally used[50]. Geological constraints on the ice sheet history [21] and GPS measurements of
133 contemporary uplift [46,51] allow GIA models to be scrutinised and calibrated. More of both these data
134 sets are needed, especially in East Antarctica. Given their apparent diversity, the spread of GIA and
135 surface mass balance models should be evaluated in concert with the satellite gravimetry, altimetry,
136 and velocity measurements. A reassessment of satellite measurements acquired during the 1990s
137 would address the imbalance that is present in the current record. Alternative techniques (e.g. [52]) for
138 the combination of satellite data sets should be explored, and satellite measurements with common
139 temporal sampling should be contrasted. The ice sheet mass balance record should now be
140 separated into the contributions due to short-term fluctuations in surface mass balance and longer-
141 term trends in glacier ice. In addition to these obvious improvements, continued satellite
142 observations are, of course, essential.

143 ## References

144 1 Fretwell, P. *et al.* Bedmap2: Improved ice bed, surface and thickness datasets for Antarctica.
145 *Cryosphere* **7**, 375-393, doi:10.5194/tc-7-375-2013 (2013).

146 2 Rignot, E., Mouginot, J. & Scheuchl, B. Ice flow of the antarctic ice sheet. *Science* **333**, 1427-
147 1430, doi:10.1126/science.1208336 (2011).

148 3 Zwally, H. J., Giovinetto, M. B., Beckley, M. A. & Saba, J. L. (GSFC Cryospheric Sciences
149 Laboratory, 2012).

150 4 Shepherd, A. *et al.* Recent loss of floating ice and the consequent sea level contribution.
151 *Geophys. Res. Lett.* **37**, doi:10.1029/2010GL042496 (2010).

5 Cook, A. J. & Vaughan, D. G. Overview of areal changes of the ice shelves on the Antarctic Peninsula over the past 50 years. *Cryosphere* **4**, 77-98, doi:10.5194/tc-4-77-2010 (2010).

6 Rignot, E., Mouginot, J., Morlighem, M., Seroussi, H. & Scheuchl, B. Widespread, rapid grounding line retreat of Pine Island, Thwaites, Smith, and Kohler glaciers, West Antarctica, from 1992 to 2011. *Geophys. Res. Lett.* **41**, 3502-3509, doi:10.1002/2014GL060140 (2014).

7 Konrad, H. *et al.* Net retreat of Antarctic glacier grounding lines. *Nat. Geosci.* **In press** (2018).

8 Joughin, I., Tulaczyk, S., Bindschadler, R. & Price, S. F. Changes in west Antarctic ice stream velocities: Observation and analysis. *J. Geophys. Res. B Solid Earth* **107**, EPM 3-1 - 3-22 (2002).

9 Rignot, E. *et al.* Accelerated ice discharge from the Antarctic Peninsula following the collapse of Larsen B ice shelf. *Geophys. Res. Lett.* **31**, L18401 18401-18404, doi:10.1029/2004GL020697 (2004).

10 Shepherd, A., Wingham, D. J. & Mansley, J. A. D. Inland thinning of the Amundsen Sea sector, West Antarctica. *Geophys. Res. Lett.* **29**, 2-1 (2002).

11 Scambos, T. A., Bohlander, J. A., Shuman, C. A. & Skvarca, P. Glacier acceleration and thinning after ice shelf collapse in the Larsen B embayment, Antarctica. *Geophys. Res. Lett.* **31**, L18402 18401-18404, doi:10.1029/2004GL020670 (2004).

12 Rignot, E. & Thomas, R. H. Mass balance of polar ice sheets. *Science* **297**, 1502-1506, doi:10.1126/science.1073888 (2002). **This paper presents the first continent-wide assessment of the Antartic ice sheet mass budget - the difference between snow input and glacier ice discharge.**

13 Wingham, D. J., Ridout, A. J., Scharroo, R., Arthern, R. J. & Shum, C. K. Antarctic elevation change from 1992 to 1996. *Science* **282**, 456-458, doi:10.1126/science.282.5388.456 (1998). **This study reports the first survey of the Antarctic ice sheet volume and mass change based on repeat satellite altimetry.**

14 Velicogna, I. & Wahr, J. Measurements of time-variable gravity show mass loss in Antarctica. *Science* **311**, 1754-1756, doi:10.1126/science.1123785 (2006). **This study presents the first assessment of Antarctic ice sheet mass change determined from satellite gravimetry.**

15 van Wessem, J. M. *et al.* Modelling the climate and surface mass balance of polar ice sheets using RACMO2, part 2: Antarctica (1979–2016). *The Cryosphere Discuss.* **2017**, 1-35, doi:10.5194/tc-2017-202 (2017).

16 King, M. A. *et al.* Lower satellite-gravimetry estimates of Antarctic sea-level contribution. *Nature* **491**, 586-589, doi:10.1038/nature11621 (2012).

17 Briggs, K. *et al.* Charting ice-sheet contributions to global sea-level rise. *Eos, Transactions American Geophysical Union* **97** (2016).

18 Shepherd, A. *et al.* A reconciled estimate of ice-sheet mass balance. *Science* **338**, 1183-1189, doi:10.1126/science.1228102 (2012). **This large scale inter-comparison exercise reports the first community assessment of the Antarctic ice sheet mass balance.**

19 Zwally, H. J., Giovinetto, M. B., Beckley, M. A. & Saba, J. L. (ed GSFC Cryospheric Sciences Laboratory) (2012).

20 Rignot, E., Mouginot, J. & Scheuchl, B. Antarctic grounding line mapping from differential satellite radar interferometry. *Geophys. Res. Lett.* **38**, doi:10.1029/2011GL047109 (2011).

21 Bentley, M. J. *et al.* A community-based geological reconstruction of Antarctic Ice Sheet deglaciation since the Last Glacial Maximum. *Quat. Sci. Rev.* **100**, 1-9, doi:10.1016/j.quascirev.2014.06.025 (2014). **This community assessment collates and reports geological evidence of the Antarctic ice sheet retreat over the current inter-glacial period, a key factor in the regional glacial isostatic adjustment.**

22 Peltier, W. R. in *Annual Review of Earth and Planetary Sciences* Vol. 32 111-149 (2004).

23 A, G., Wahr, J. & Zhong, S. Computations of the viscoelastic response of a 3-D compressible earth to surface loading: An application to glacial isostatic adjustment in Antarctica and Canada. *Geophys. J. Int.* **192**, 557-572, doi:10.1093/gji/ggs030 (2013).

24 Sasgen, I. *et al.* Antarctic ice-mass balance 2003 to 2012: Regional reanalysis of GRACE satellite gravimetry measurements with improved estimate of glacial-isostatic adjustment based on GPS uplift rates. *Cryosphere* **7**, 1499-1512, doi:10.5194/tc-7-1499-2013 (2013).

25 Peltier, W. R., Argus, D. F. & Drummond, R. Space geodesy constrains ice age terminal deglaciation: The global ICE-6G-C (VM5a) model. *J. Geophys. Res. B Solid Earth* **120**, 450-487, doi:10.1002/2014JB011176 (2015).

26 King, M. A., Whitehouse, P. L. & van der Wal, W. Incomplete separability of Antarctic plate rotation from glacial isostatic adjustment deformation within geodetic observations. *Geophys. J. Int.* **204**, 324-330, doi:10.1093/gji/ggv461 (2016).

27 Whitehouse, P. L., Bentley, M. J., Milne, G. A., King, M. A. & Thomas, I. D. A new glacial isostatic adjustment model for Antarctica: Calibrated and tested using observations of relative sea-level change and present-day uplift rates. *Geophys. J. Int.* **190**, 1464-1482, doi:10.1111/j.1365-246X.2012.05557.x (2012).

28 Spada, G., Melini, D. & Colleoni, F. (ed geodynamics.org) (2015).

29 Konrad, H., Sasgen, I., Pollard, D. & Klemann, V. Potential of the solid-Earth response for limiting long-term West Antarctic Ice Sheet retreat in a warming climate. *Earth Plan. Sci. Lett.* **432**, 254-264, doi:10.1016/j.epsl.2015.10.008 (2015).

30 Briggs, R. D., Pollard, D. & Tarasov, L. A data-constrained large ensemble analysis of Antarctic evolution since the Eemian. *Quat. Sci. Rev.* **103**, 91-115, doi:10.1016/j.quascirev.2014.09.003 (2014).

31 Ivins, E. R. & James, T. S. Antarctic glacial isostatic adjustment: A new assessment. *Antarct. Sci.* **17**, 541-553, doi:10.1017/S0954102005002968 (2005).

32 Ivins, E. R. *et al.* Antarctic contribution to sea level rise observed by GRACE with improved GIA correction. *J. Geophys. Res. B Solid Earth* **118**, 3126-3141, doi:10.1002/jgrb.50208 (2013).

33 Nield, G. A. *et al.* Rapid bedrock uplift in the Antarctic Peninsula explained by viscoelastic response to recent ice unloading. *Earth Plan. Sci. Lett.* **397**, 32-41, doi:10.1016/j.epsl.2014.04.019 (2014).

34 Mouginot, J., Rignot, E. & Scheuchl, B. Sustained increase in ice discharge from the Amundsen Sea Embayment, West Antarctica, from 1973 to 2013. *Geophys. Res. Lett.* **41**, 1576-1584, doi:10.1002/2013GL059069 (2014).

35 Shepherd, A., Fricker, H. A. & Farrell, S. L. The state of Antarctic ice. *Nature* **In press** (2018).

36 Boening, C., Lebsock, M., Landerer, F. & Stephens, G. Snowfall-driven mass change on the East Antarctic ice sheet. *Geophys. Res. Lett.* **39**, doi:10.1029/2012GL053316 (2012).

37 Medley, B. *et al.* Temperature and Snowfall in Western Queen Maud Land Increasing Faster Than Climate Model Projections. *Geophys. Res. Lett.* **45**, 1472-1480, doi:10.1002/2017GL075992 (2018).

38 Favier, V. *et al.* An updated and quality controlled surface mass balance dataset for Antarctica. *Cryosphere* **7**, 583-597, doi:10.5194/tc-7-583-2013 (2013).

39 Van De Berg, W. J. & Medley, B. Brief Communication: Upper-air relaxation in RACMO2 significantly improves modelled interannual surface mass balance variability in Antarctica. *Cryosphere* **10**, 459-463, doi:10.5194/tc-10-459-2016 (2016).

40 Palerme, C. *et al.* Evaluation of Antarctic snowfall in global meteorological reanalyses. *Atmos. Res.* **190**, 104-112, doi:10.1016/j.atmosres.2017.02.015 (2017).

41 Van Wessem, J. M. *et al.* Improved representation of East Antarctic surface mass balance in a regional atmospheric climate model. *J. Glaciol.* **60**, 761-770, doi:10.3189/2014JoG14J051 (2014).

42 Bromwich, D. H., Nicolas, J. P. & Monaghan, A. J. An Assessment of precipitation changes over antarctica and the southern ocean since 1989 in contemporary global reanalyses. *J. Clim.* **24**, 4189-4209, doi:10.1175/2011JCLI4074.1 (2011).

253 43 Behrangi, A. *et al.* Status of high-latitude precipitation estimates from observations and
254 reanalyses. *J. Geophy. Res.* **121**, 4468-4486, doi:10.1002/2015JD024546 (2016).
255 44 Klemann, V. & Martinec, Z. Contribution of glacial-isostatic adjustment to the geocenter
256 motion. *Tectonophysics* **511**, 99-108, doi:10.1016/j.tecto.2009.08.031 (2011).
257 45 van der Wal, W., Whitehouse, P. L. & Schrama, E. J. O. Effect of GIA models with 3D
258 composite mantle viscosity on GRACE mass balance estimates for Antarctica. *Earth Plan. Sci.*
259 *Lett.* **414**, 134-143, doi:10.1016/j.epsl.2015.01.001 (2015).
260 46 Martín-Español, A. *et al.* An assessment of forward and inverse GIA solutions for Antarctica.
261 *J. Geophys. Res. B Solid Earth* **121**, 6947-6965, doi:10.1002/2016JB013154 (2016).
262 47 Caron, L. *et al.* GIA Model Statistics for GRACE Hydrology, Cryosphere, and Ocean Science.
263 *Geophys. Res. Lett.*, doi:10.1002/2017GL076644 (2018).
264 48 Medley, B. *et al.* Constraining the recent mass balance of pine island and thwaites glaciers,
265 west antarctica, with airborne observations of snow accumulation. *Cryosphere* **8**, 1375-1392,
266 doi:10.5194/tc-8-1375-2014 (2014).
267 49 Lewis, G. *et al.* Regional Greenland accumulation variability from Operation IceBridge
268 airborne accumulation radar. *Cryosphere* **11**, 773-788, doi:10.5194/tc-11-773-2017 (2017).
269 50 Thomas, E. R. *et al.* Regional Antarctic snow accumulation over the past 1000 years. *Climate*
270 *of the Past* **13**, 1491-1513, doi:10.5194/cp-13-1491-2017 (2017).
271 51 Thomas, I. D. *et al.* Widespread low rates of Antarctic glacial isostatic adjustment revealed
272 by GPS observations. *Geophys. Res. Lett.* **38**, doi:10.1029/2011GL049277 (2011).
273 52 Wahr, J., Wingham, D. & Bentley, C. A method of combining ICESat and GRACE satellite data
274 to constrain Antarctic mass balance. *J. Geophys. Res. B Solid Earth* **105**, 16279-16294 (2000).
275

Supplementary Information

A table summarising the details of the satellite datasets is included as Supplementary Information (Supplementary Information Table 1).

Acknowledgements

This work is an outcome of the ESA-NASA Ice Sheet Mass Balance Inter-comparison Exercise. Andrew Shepherd was additionally supported by a Royal Society Wolfson Research Merit Award.

Author Contributions

Andrew Shepherd and Erik Ivins designed and led the study. Eric Rignot, Ben Smith, Michiel van den Broeke, Isabella Velicogna, and Pippa Whitehouse led the input-output, altimetry, surface mass balance, gravimetry, and glacial isostatic adjustment experiments, respectively. Gorka Moyano and Mark Pattle performed the data collation and analysis. Andrew Shepherd, Erik Ivins, Kate Briggs, Gerhard Krinner, Martin Horwath, Ian Joughin, Hannes Konrad, Malcolm McMillan, Jeremie Mouginot, Sophie Nowicki, Inès Otosaka, Mark Pattle, Tony Payne, Eric Rignot, Ingo Sasgen, Ted Scambos, Nicole Schlegel, Tom Slater, Ben Smith, Isabella Velicogna, Melchior van Wessem, and Pippa Whitehouse wrote and edited the manuscript. All authors participated in the data interpretation and commented on the manuscript.

Author Information

Reprints and permissions information is available at www.nature.com/reprints. The authors declare no competing interests. Correspondence and requests for materials should be addressed to a.shepherd@leeds.ac.uk.

Tables

Region	1992-1997 (Gt/year)	1997-2002 (Gt/year)	2002-2007 (Gt/year)	2007-2012 (Gt/year)	2012-2017 (Gt/year)	1992-2011 (Gt/year)	1992-2017 (Gt/year)
EAIS	11 ± 58	8 ± 56	12 ± 43	23 ± 38	-28 ± 30	13 ± 50	5 ± 46
WAIS	-53 ± 29	-41 ± 28	-65 ± 27	-148 ± 27	-159 ± 26	-73 ± 28	-94 ± 27
APIS	-7 ± 13	-6 ± 13	-20 ± 15	-35 ± 17	-33 ± 16	-16 ± 14	-20 ± 15
AIS	-49 ± 67	-38 ± 64	-73 ± 53	-160 ± 50	-219 ± 43	-76 ± 59	-109 ± 56

Table 1 | Rates of ice sheet mass change. Rates were determined from all satellite measurements over various epochs for the East Antarctic (EAIS), West Antarctic (WAIS), Antarctic Peninsula (APIS) and Antarctic (AIS) ice sheets. The period 1992-2011 is included for comparison to a previous assessment [18], which reported mass balance estimates of 14 **±** 43 Gt/yr for the EAIS, -65 ± 26 Gt/yr for the WAIS, -20 ± 14 Gt/yr for the APIS, and -71 ± 53 Gt/yr for the AIS. The small differences in our updated estimates are due to increases in the datasets used.

Figure Legends

Figure 1. Antarctic ice sheet mass balance. Rate of mass change of the Antarctic Peninsula (a), West Antarctic Ice Sheet (b), and East Antarctic Ice Sheet (c) as determined from satellite altimetry (red), input-output (blue), and gravimetry (green) observations and an average of estimates across each class of measurement technique (black) The estimated one-, two-, and three-sigma range of the

class average are shaded in dark, mid, and light grey, respectively, and the number of individual mass balance estimates collated at each epoch is shown along the top of each chart.

Figure 2. Cumulative Antarctic ice sheet mass change. Cumulative ice sheet mass changes (solid lines) are determined from the integral of the measurement class average (Figure 1) for each ice sheet. The estimated one-sigma uncertainty of the cumulative change is shaded.

Methods

Data

We analyse five groups of data; mass balance estimates determined from satellite altimetry, gravimetry, and the input-output method, and model estimates of surface mass balance and glacial isostatic adjustment. The data sets are computed using common spatial and temporal domains to facilitate their aggregation, and according to methods report in the peer reviewed literature. In total 24 individual mass balance data sets were included. The data include 25 years of satellite radar altimeter measurements, 24 years of satellite input-output method measurements, and 14 years of satellite gravimetry measurements (Extended Data Figure 1). Among these data are estimates of ice sheet mass balance for each ice sheet derived from each satellite technique. In comparison to the first IMBIE assessment, new satellite missions, updated methodologies and improvements in geophysical corrections have contributed to an increase in the quantity, duration and overlap period of data used in this second assessment. In addition, two new experiment groups have assessed 11 Glacial Isostatic Adjustment models and 4 Surface Mass Balance models. The complete list of data sets can be found in Supplementary Information Table 1.

Drainage Basins

In this assessment, we analyse mass trends using two sets of ice sheet drainage basin (Extended Data Figure 2), to ensure consistency with those used in the first IMBIE assessment [18], and to evaluate an updated definition tailored towards input-output method assessments. The first drainage basin set was delineated using surface elevation maps derived from ICESat-1 based on the provenance of the ice, and includes 27 basins [3]. The second set are updated to consider other factors such as the direction of ice flow, and include 18 basins in Antarctica [2,20]. To assess the effect of the different basin outline sets on the estimates of ice sheet mass balance, we compared mass balance determinations between the two delineations of ice sheet drainage basins. This evaluation was facilitated by seven estimates (altimetry or gravimetry) determined using both drainage basin sets. At the scale of the major ice sheet divisions, the delineations produce similar total extents. By far the largest differences occur in the delineation (or definition) of East and West Antarctica, due to differences in the position of the ice divide separating them. Within these regions, the root mean-square difference between 26 pairs of ice sheet mass balance estimates computed using the two drainage basin sets is 8.7 Gt/yr. This difference is small in comparison to the certainty of individual ice sheet mass balance assessments.

Computing Rates of Mass Change

The raw satellite mass balance data are either time-series of either relative mass change, $\Delta M(t)$, or the rate of mass change, $dM(t)/dt$, plus their associated uncertainty, integrated over at least one of the ice sheet regions defined in the standard drainage basin sets. In the case of $\Delta M(t)$, the time series represents the change in mass through time relative to some nominal reference value. The duration and sampling frequency of the time-series was not restricted. In practice, few mass time-series were of $\Delta M(t)$ *and* $dM(t)/dt$. Because the inter-comparison exercise is based on comparing and aggregating rates of mass change, $dM(t)/dt$, a common solution was implemented to derive $dM(t)/dt$ values from data sets that comprised $\Delta M(t)$ only. Each $\Delta M(t)$ time series was used to

generate a time-varying estimate of the rate of mass change, d(ΔM(t))/dt=dM(t)/dt, and an estimate of the associated uncertainty, using a consistent approach. Time varying rates of mass change were computed by applying a sliding fixed-period window to the ΔM(t) time series. At each node, defined by the sampling period of the input time series, dM(t)/dt and its standard error, $\sigma_{dM(t)/dt}$, were estimated by fitting a linear trend to data within the window using a weighted least-squares approach, with each point weighted by its respective error variance, $\sigma_{\Delta M(t)}^2$. The regression error, $\sigma_{dM(t)/dt}$, incorporates measurement errors and model structural error due to any variability that deviates from linear trends in ice mass, and may be a conservative estimate in locations where such deviation is present. Time series of dM(t)/dt computed using this approach were truncated by half the moving average window period. When integrated, the dM(t)/dt time series correspond to a low-pass filtered version of the original ΔM(t) time-series. Although the current linear regression assumes uncertainties are uncorrelated, the smoothing we apply during the trend calculation does cause data points to be correlated during a number of epochs beyond the sliding window.

Surface Mass Balance

Ice sheet surface mass balance (SMB) comprises a variety of processes governed by the interaction of the superficial snow and firn layer with the atmosphere. A direct mass exchange occurs via precipitation and surface sublimation. Snow drift and the formation of meltwater and its subsequent refreezing or retention redistribute mass spatially or lead to further mass loss via erosion and sublimation, or runoff. In this assessment, a range of SMB products are compared. Four SMB model solutions were considered for Antarctica (Extended Data Table 1); two regional models - RACMO2.3 [41] and MARv3.6 [53] - and two global reanalysis products - JRA55 [54] and ERA-Interim [55]. The two regional climate models agree well in terms of their spatially integrated SMB, apart from the Peninsula where there is an offset of about 10 Gt/month between them (Extended Data Figure 3). However, the reanalysis data underestimated the average SMB compared to the regional climate models by 200 to 350 Gt/yr. The SMB assessment illustrates that products of similar class (climate

379 models, reanalysis product) agree well, suggesting that groupings of their output may be
380 appropriate. Model resolution is, however, found to be an important factor when estimating SMB
381 and its components, as respective contributions where only the spatial resolution differed yield
382 regional differences.

383 ## Glacial Isostatic Adjustment

384 Glacial isostatic adjustment (GIA) is the delayed response of the solid Earth to changes in time-
385 variable surface loading through the growth and decay of ice sheets, and associated changes in sea
386 level. Because GIA contributes to changes in the ice sheet surface elevation and gravity field, it must
387 be accounted for in measurements of the change in elevation and gravity for the purpose of isolating
388 the contribution solely caused by ice sheet imbalance. In this assessment, we compare different
389 solutions derived from continuum-mechanical forward modelling to inform the interpretation of the
390 satellite altimetry and gravimetry data which depend on the correction, and to advise future
391 assessment exercises. Twelve GIA contributions were received covering Antarctica (Extended Data
392 Table 2), ten of which are global [23-30,32] and two of which are regional models [33]. As a broad array of
393 data may be used to constrain GIA forward models, we anticipate spread in the predictions.

394 In the present analysis, the degree of similarity between the various GIA model solutions is assessed.
395 Areas of enhanced present-day vertical surface motion and (dis-)agreement between contributions
396 have been identified by averaging the uplift rates over the contributions and computing respective
397 standard deviations (Extended Data Figure 4). In some cases, it was necessary to estimate the GIA
398 contribution to gravimetric mass trends; this was done using common geographical masks and
399 truncation, and a standardized treatment of low degree harmonics. In Antarctica, the Amundsen Sea
400 sector and the regions covered by the Ross and Filchner Ronne Ice Shelves stand out as having both
401 high uplift rates (5-7 mm/yr on average) and high variability in uplift rates (peaking at >10 mm/yr
402 standard deviation in the Amundsen sector) among the models considered. Elsewhere in coastal
403 regions, uplift occurs at more moderate rates (~2 mm/yr on average), and the interior of East

Antarctica exhibits slow subsidence. In these regions, the average signal is accompanied by relatively low variance among the GIA models (0-1.5 mm/yr standard deviation). None of the models fully capture portions of the uplift that are observed to be very large (e.g. [56]), hence, we can anticipate a bias toward low values for the GIA correction averaged over such regions. In areas of low mantle viscosity, however, such as part of the WAIS, the LGM-related GIA signal may be over-predicted, and it is not clear whether a bias exists at the continental scale.

Differences between the model predictions arise for a variety of additional reasons. Technical differences in the modelling approach, for example relating to the consideration of self-gravitation, ocean loading, rotational feedback, and compressibility, will be most important at the global scale, but may explain only small differences among the regional models. Differing treatment of ice/ocean loading in regions that have experienced marine-based grounding line retreat during the last glacial cycle may explain the differences in model predictions for the ICE_6G_C/VM5a combination (see Supplementary Information Table 1). Some small differences should be expected when comparing models that use spherical harmonic and finite element approaches. Looking beyond consideration of the model physics, larger differences arise due to the various approaches used to determine the two principal unknowns associated with forward modelling of GIA, namely ice history and Earth rheology. There is no generally accepted 'best approach' to determining these inputs, and indeed useful advances can be made by comparing the results of complementary approaches. In the models considered here, approaches to determining the ice history include dynamical ice-sheet modelling, coupled ice-sheet–GIA modelling, tuning to fit geodetic constraints, tuning to fit geological constraints, and use of direct observations of historical ice sheet change. When defining the rheological properties of the solid Earth, most studies have opted to use a Maxwell rheology to define a radially-symmetric Earth, but the use of a power-law rheology and/or fully-3D Earth model to capture the spatial complexity of mantle properties is increasingly popular. An intermediate approach used in many of the data sets included in this study has been to develop a regional GIA model that reflects local Earth structure. Such models can be tuned, albeit imperfectly, to provide as

accurate a representation of GIA in that region as is possible. However, it remains a difficult and important challenge to incorporate these regional studies into a global framework. Finally, although four of the considered GIA models do provide a measure of uncertainty, and a number of studies have used an ensemble modelling approach [24,30], an important future goal for the GIA modelling community is the inclusion of robust error estimates for all model predictions.

To compare the GIA models, Stokes coefficients relating to their gravitational signal were used to determine the approximate magnitude of the effect of applying each correction to GRACE data (Extended Data Table 2). This is a preliminary assessment, because the effect of applying a GIA correction depends also on the methods used to process the GRACE data. Moreover, an agreement on the modelling of the rational feedbacks has so far not been reached within the GIA community, leading to a large spread in the modeled degree 2 coefficients and possibly a strong bias when a correction is applied that is inconsistent with the GRACE observations (up to ca. 40 Gt/yr). In addition, none of the current GIA data sets include estimates of the GIA-induced geocenter motion (degree 1 coefficients). Therefore, we omit degree 1 and 2 coefficients in this assessment of the GIA-induced apparent mass change at this stage. From models representing GIA in Antarctic only, we estimate that this omission may change the apparent mass change value by up to 20 %, which is currently not included in the GIA error budget. There is relatively good agreement between the ten models that cover all of Antarctica (Extended Data Table 2); the estimated GIA contribution ranges from +12 to +81 Gt/yr, and the mean value is 56 Gt/yr. Although van der Wal et al. is a notable outlier, this is the only solution to account for 3D variations in Earth rheology, and it will be interesting to compare this result with other such models that are in development. It is important to note that two of the GIA models are regional (Nield, Barletta); although they cannot be directly compared with the continental-scale models, the magnitude of their signals is nonetheless included for interest.

Mass Balance Intra-comparison

First, we compare estimates of mass change within each of the three geodetic technique experiment groups, separately, to assess the degree to which results from common techniques concur and to then arrive at individual, aggregated estimates of mass change derived from each technique alone. In each case we compare estimated rates of mass change derived from a common technique over a common geographical region and over the full period of the respective data sets. Where data sets were computed using both drainage basin definitions, the arithmetic mean of the two estimates is presented. This is justified because the choice of drainage basin set has a very small (<10 Gt/yr) impact on estimates of mass balance at the ice sheet scale and even less at the regional scale. Within each experiment group, we perform an unweighted average of all individual data to obtain a single estimate of the rate of mass change per ice sheet for each geodetic technique In a few cases, it was not possible to determine time-varying rates of mass change from individual estimates, because only constant rates of mass change and constant cumulative mass changes were supplied. Although the effect of averaging these data sets with time-varying solutions is to dampen the temporal variability present within the series of finer resolution, they are retained for completeness. We estimate the uncertainty of the average mass trends emerging from each experiment group as the average of the errors associated with each individual estimate at each epoch.

To aid comparison, we (i) computed time-variable rates of mass change and their associated uncertainty over successive 36-month periods stepped in 1-month intervals from time-varying cumulative mass changes, and we then (ii) average rates of mass change over 1-year periods to remove signals associated with seasonal cycles. Time-varying rates of mass change are truncated at the start and end of each series to reflect the half-width of the time interval over which rates are computed, though this period is recovered on integration to cumulative mass changes. The extent to which we are able to analyse differences in mass balance solutions emerging from common satellite approaches is limited by the mismatch in temporal resolution of the individual datasets, which makes methodological and sampling differences difficult to separate.

Gravimetry Mass Balance Intra-comparison

Within the gravimetry experiment group, 15 estimates of mass balance derived from the GRACE satellites were assessed, in entirety spanning the period July 2002 to September 2016. Of these datasets, four (Luthcke, Moore, Save, Wiese) are derived with direct imposition of the GRACE Level-1 K-band range-data [57-60]. These impositions result in 4 different, and quite independently derived, mascon approaches. Other methods often refer to 'mascon analysis', but are conducted on post-spherical harmonic (post-SH) expansions and without imposing the Level 1 K-band range data. We distinguish the later methods, referring to them as 'post-SH mascons'. Eleven contributions are derived from monthly spherical harmonic solutions of the global gravity field using somewhat different approaches [61-67], which can be loosely classified as region integration approaches for 3 contributions (Blazquez, Groh, Horvath), post-SH mascon approaches for 4 contributions (Bonin, Forsberg, Schrama, Velicogna). Forward-modelling is also an approach used in two contributions (Wouters, Seo) and this essentially involves modelling of mass change with iterative comparison to the GRACE-derived signal. One estimate (Harig) uses Slepian functions [68]. One esimate (Rietbroek) uses a hybrid approach involving satellite altimetry that does not fall within the above categories [69]; although these results are excluded from our gravimetry-only average, we present them alongside the gravimetry-only results for comparison. No restrictions were imposed on the choice of glacial isostatic adjustment correction, and among the GRACE solutions we consider six different models were used for this purpose [22,25,27,31,32,44]. We did, however, assess a wider set of nine continent-wide forward models and two regional models to better understand uncertainties in the GIA signal itself.

In total, there were 15 estimates of mass balance for each of the APIS, WAIS, and EAIS. All were time-varying cumulative mass change solutions - the primary GRACE observable - and we computed time-varying rates of mass change from these data. Combining all of the individual mass balance estimates, the effective (average) temporal resolution of the aggregated solution is 1 year. Further details of the gravimetry data sets and methods are included in Supplementary Information Table 1.

Extended Data Figure 5 shows a comparison of rates of mass change obtained from all gravimetry mass balance solutions, calculated over the three main ice sheet regions. At individual epochs, differences between time-varying rates of mass change are generally smaller than 50 Gt/yr in each ice sheet region, and typically fall in the range 10 to 20 Gt/yr. Over the full period of the data, individual rates of mass balance for the APIS, WAIS, and EAIS vary between -80 to +10, -260 to -20, and -120 to +200 Gt/yr, respectively. Considering all of the gravimetry data (Extended Data Table 3); the standard deviation of mass trends estimated during the period 2005 to 2015 is less than 24 Gt/yr in all three ice sheet regions, with the largest spread occurring in the EAIS. In all three ice sheet regions, the spread of individual mass balance estimates is well represented by the mean considering the uncertainties of the individual and aggregated datasets.

Altimetry Mass Balance Intra-comparison

We assessed 7 radar and laser altimetry derived estimates of Antarctic ice sheet mass balance data sets, in entirety spanning the period April 1992 to July 2017. In total, 6 estimates of mass change were for the APIS, 7 for the EAIS, and 7 for the WAIS. Of these, 4 included data from radar altimetry, and 6 from laser altimetry. A variety of different techniques were employed to arrive at elevation and mass trends [70-76]. Only 2 of the altimetry data sets were time-series of cumulative mass change, from which we computed time-varying rates of mass change. The remaining altimetry data sets were constant rates of mass change, which appear in our altimetry average as time-invariant solutions. The period over which altimetry rates of mass change were computed ranged from 2 to 24 years. In consequence, the aggregated dataset has a temporal resolution that is lower than annual. Including all individual mass balance data sets, the effective (average) temporal resolution of the aggregated solution is 3.3 years. Further details of the altimetry data sets and methods are included in Supplementary Information Table 1.

With a few exceptions, rates of mass change determined from radar and laser altimetry tend to differ by less than 100 Gt/yr at all times in each ice sheet region (Extended Data Figure 5). The main

exceptions are in the EAIS, where one estimate (Zwally) reports mass trends that are ~100 Gt/yr more positive than all others during the ERS and ICESat periods and the WAIS, where two estimates (Zwally and Helm) report rates that are ~70 Gt/yr less negative than the others during the ICESat period. Among the remaining data sets, the closest agreement occurs at the APIS, where mass trends agree to within 30 Gt/yr at all times, and the poorest agreement occurs at the EAIS, where mass trends depart by up to 100 Gt/yr. The largest differences are among datasets that are constant in time during periods where rapid changes in mass balance occur in the annually resolved time series, suggesting that a proportion of the difference is due to their poor temporal resolution. Mass balance solutions from the relatively short (six-year) ICESat mission also appear to show larger spreads compared to those determined from longer (decade-scale) radar-altimetry missions. This larger spread is due in part to differences in the bias-correction models applied to ICESat data [75,77-79] and in part to the large influence of firn densification on altimetry measurements over short periods, which have been corrected for using different models. Firn-densification models are generally not applied to mass balance solutions determined from radar altimetry. Further analysis of the corrections for bias between ICESat campaigns and firn compaction is required to establish the significance of the differences and to reduce their collective uncertainty. Comparing rates of mass change (Extended Data Table 3), the average standard deviation of all mass trends at each epoch over the common period 2005 to 2015 is less than 54 Gt/yr in all four ice sheet regions. The largest spread among the individual values occurs in the EAIS. Other than this sector, all of the individual estimates lie close to the ensemble average, considering the respective uncertainty of the measurements.

Input-Output Method Intra-comparison

Although the input-output method is a most direct measure of changing in mass fluxes, a main difficulty is that it must differ two large numbers - one for annual SMB and the other for discharge plus grounding line migrations - *and* deal appropriately with the error budgets of both, in order to assess mass balance. A consequence of this complexity is that few input-output method data sets

556 exist at the ice sheet scale. In this assessment, we collate just two input-output data sets, both based
557 on the same method [80] - far fewer than were considered for altimetry and gravimetry. The first
558 input-output method dataset spans the period 1992 to 2010 [18]. The second input-output method
559 dataset is limited to the period 2002 to 2016. The same SMB model was used in both assessments -
560 RACMO2.3. Further details of the input-output method data sets and methods are included in
561 Supplementary Information Table 1.

562 We compared the two input-output method data sets during the period 2002 to 2010 when they
563 overlap (Extended Data Table 3). The smallest differences (up to 30 Gt/yr) arise in the APIS and the
564 WAIS, and the largest differences (up to 70 Gt/yr) occur at the EAIS. In all cases, the average
565 difference between estimates of mass balance derived from each dataset is comparable to the
566 estimated certainty. Including both datasets, rates of mass balance over the period 1992 to 2016 for
567 the APIS, WAIS and EAIS fall in the range -125 to +25 Gt/yr, -300 to +100 Gt/yr and -200 to +200
568 Gt/yr, respectively (Extended Data Figure 5). The origin of the differences between the two datasets
569 requires further investigation.

570 Ice Sheet Mass Balance Inter-comparison

571 To assess the degree to which the satellite techniques concur, we used the aggregated time series
572 emerging from each geodetic technique experiment group to compute changes in ice sheet mass
573 balance within common geographical regions and over a common interval of time (the overlap
574 period). The aggregated time series were calculated as the arithmetic mean of all available rates of
575 ice sheet mass balance derived from the same satellite technique at each available epoch. We used
576 the individual ice sheets and their integrals as common geographical regions. The maximum duration
577 of the overlap period is limited to the 14-year interval when all three satellite techniques were
578 optimally operational, namely 2002 to 2016. However, we also considered the availability of mass
579 balance data sets, which leads us to select the period 2003 to 2010 as the optimal interval (see
580 Figure 1). When the aggregated mass balance data emerging from all three experiment groups are

581 degraded to a common temporal resolution of 36 months, the time-series are on average well
582 correlated ($0.5<r^2<0.9$) at the APIS and WAIS. At the EAIS, however, the aggregated altimetry mass
583 balance time series are poorly correlated ($r^2<0.1$) in time with the aggregated gravimetry and input-
584 output method data. Possible explanations for this include the relatively high short-term variability
585 in mass fluctuations in this region, the relatively low trend in mass, and the heterogeneous temporal
586 resolution of the aggregated altimetry data set. Over longer periods, marked increases in the rate of
587 mass loss from the WAIS are also recorded in all three satellite data sets.

588 Because the comparison period is long in relation to the timescales over which surface mass balance
589 fluctuations typically occur, their potential impact on the overall inter-comparison is reduced. The
590 closest agreement between individual estimates of ice sheet mass balance occurs at the APIS and
591 the WAIS, where the standard deviation across all techniques falls between 15 and 41 Gt/yr
592 (Extended Data Table 4). The greatest departure occurs at the EAIS, where the input-output method
593 and gravimetry estimates of mass balance differ by ~80 Gt/yr, and where the standard deviation of
594 all three estimates is ~40 Gt/yr. This high degree of variance is expected due to the relatively large
595 size of the region, small amplitude of signals and poor independent controls on coastal SMB. When
596 compared to the mean, there are no significant differences between estimates of ice sheet mass
597 balance determined from the individual satellite techniques and, in contrast to the first assessment,
598 this finding also holds at continental and global scale. We conclude, therefore, that estimates of
599 mass balance determined from independent geodetic techniques agree when compared to their
600 respective uncertainties.

601 Several noteworthy patterns in the distribution of mass balance estimates determined during the
602 overlap period (2003 to 2010) merit further discussion. Estimates of mass balance derived from
603 satellite altimetry and gravimetry are agree to within 15 Gt/yr, on average, and with the mean of all
604 three techniques, in all ice sheet regions. In contrast, estimates of mass balance determined from
605 the input-output method are 55 Gt/yr more negative, on average, than the mean in all ice sheet

606 regions. However, despite the bias, the input-output method estimates remain in agreement
607 because their estimated uncertainty is relatively large (approximately three times larger than that of
608 the other techniques). A more detailed analysis of the primary and ancillary datasets is required to
609 establish whether this bias is significant or systematic.

610 Ice Sheet Mass Balance Integration

611 We combined estimates of ice-sheet mass balance derived from each geodetic technique
612 experiment group to produce a single, *reconciled* assessment, following the same approach as the
613 first assessment exercise. This was computed as the arithmetic mean of the average rates of mass
614 change derived from each experiment group, within the regions of interest and at the time periods
615 for which the experiment group mass trends were determined. We estimated the uncertainty of the
616 mass balance data using the following approach. Within each experiment group, the uncertainty of
617 mass trends was estimated as the average of the errors associated with each individual estimate.
618 The uncertainty of *reconciled* rates of mass change (e.g. Table 1) was estimated as the root mean
619 square of the uncertainties associated with mass trends emerging from each experiment group.
620 When summing mass trends of multiple ice sheets, the combined uncertainty was estimated as the
621 root sum square of the uncertainties for each region. Finally, to estimate the cumulative uncertainty
622 of mass changes over time, we weighted the annual uncertainty by $1/\sqrt{n}$, where n is the number of
623 years elapsed relative to the start of each time series, and then summed the weighted annual
624 uncertainties over time [81].

625 Across the full 25-year survey, the average rates of mass balance of the AIS was -109 ± 56 (Table 1).
626 To investigate inter-annual variability, we also calculated mass trends during successive 5-year
627 intervals. While the APIS and WAIS each lost mass throughout the entire survey period, the EAIS
628 experienced alternate periods of mass loss and mass gain, likely driven by inter-annual fluctuations
629 in SMB. The rate of mass loss from the WAIS has increased over time due to accelerated ice
630 discharge in the Amundsen Sea sector [34,48,74,82-84]. The most significant rise – a twofold increase in the

rate of ice loss - occurred between the periods 2002-2007 and 2007-2012 (Table 1). Overall, the WAIS accounts for the vast majority of ice mass losses from Antarctica. At the APIS, rates of ice mass loss since the early 2000's are notably higher than during the previous decade, consistent with observations of surface lowering [72,74] and increased ice flow in southerly glacier catchments [85]. The approximate state of balance of the wider EAIS suggests that the reported dynamic thinning of the Totten and Cook glaciers [86,87] has been offset by accumulation gains elsewhere [88].

Methods References

53 Fettweis, X. *et al.* Estimating the Greenland ice sheet surface mass balance contribution to future sea level rise using the regional atmospheric climate model MAR. *Cryosphere* **7**, 469-489, doi:10.5194/tc-7-469-2013 (2013).

54 Kobayashi, S. *et al.* The JRA-55 reanalysis: General specifications and basic characteristics. *J. Meteorol. Soc. Jpn.* **93**, 5-48, doi:10.2151/jmsj.2015-001 (2015).

55 Dee, D. P. *et al.* The ERA-Interim reanalysis: Configuration and performance of the data assimilation system. *Q. J. R. Meteorol. Soc.* **137**, 553-597, doi:10.1002/qj.828 (2011).

56 Groh, A. & Horwath, M. The method of tailored sensitivity kernels for GRACE mass change estimates. *Geophys. Res. Abstr.* **18**, 2016 (2016).

57 Luthcke, S. B. *et al.* Antarctica, Greenland and Gulf of Alaska land-ice evolution from an iterated GRACE global mascon solution. *J. Glaciol.* **59**, 613-631, doi:10.3189/2013JoG12J147 (2013).

58 Andrews, S. B., Moore, P. & King, M. A. Mass change from GRACE: A simulated comparison of Level-1B analysis techniques. *Geophys. J. Int.* **200**, 503-518, doi:10.1093/gji/ggu402 (2015).

59 Save, H., Bettadpur, S. & Tapley, B. D. High-resolution CSR GRACE RL05 mascons. *J. Geophys. Res. B Solid Earth* **121**, 7547-7569, doi:10.1002/2016JB013007 (2016).

60 Watkins, M. M., Wiese, D. N., Yuan, D. N., Boening, C. & Landerer, F. W. Improved methods for observing Earth's time variable mass distribution with GRACE using spherical cap mascons. *J. Geophys. Res. B Solid Earth* **120**, 2648-2671, doi:10.1002/2014JB011547 (2015).

61 Barletta, V. R., Sørensen, L. S. & Forsberg, R. Scatter of mass changes estimates at basin scale for Greenland and Antarctica. *Cryosphere* **7**, 1411-1432, doi:10.5194/tc-7-1411-2013 (2013).

62 Schrama, E. J. O., Wouters, B. & Rietbroek, R. A mascon approach to assess ice sheet and glacier mass balances and their uncertainties from GRACE data. *J. Geophys. Res. B Solid Earth* **119**, 6048-6066, doi:10.1002/2013JB010923 (2014).

63 Seo, K. W. *et al.* Surface mass balance contributions to acceleration of Antarctic ice mass loss during 2003-2013. *J. Geophys. Res. B Solid Earth* **120**, 3617-3627, doi:10.1002/2014JB011755 (2015).

64 Velicogna, I., Sutterley, T. C. & Van Den Broeke, M. R. Regional acceleration in ice mass loss from Greenland and Antarctica using GRACE time-variable gravity data. *Geophys. Res. Lett.* **41**, 8130-8137, doi:10.1002/2014GL061052 (2014).

65 Wouters, B., Bamber, J. L., Van Den Broeke, M. R., Lenaerts, J. T. M. & Sasgen, I. Limits in detecting acceleration of ice sheet mass loss due to climate variability. *Nat. Geosci.* **6**, 613-616, doi:10.1038/ngeo1874 (2013).

66 Blazquez, A. *et al.* Exploring the uncertainty in GRACE estimates of the mass redistributions at the Earth surface. Implications for the global water and sea level budgets. *Geophys. J. Int.* (In review).

67 Horvath, A. G. Vol. DGK Reihe C-803 *DGK Reihe C* 159 (Verlag der Bayerischen Akademie der Wissenschaften, München, 2017).

68 Harig, C. & Simons, F. J. Mapping Greenland's mass loss in space and time. *Proc. Natl. Acad. Sci. U. S. A.* **109**, 19934-19937, doi:10.1073/pnas.1206785109 (2012).

69 Rietbroek, R., Brunnabend, S. E., Kusche, J. & Schröter, J. Resolving sea level contributions by identifying fingerprints in time-variable gravity and altimetry. *J. Geodyn.* **59-60**, 72-81, doi:10.1016/j.jog.2011.06.007 (2012).

70 Babonis, G. S., Csatho, B. & Schenk, T. (eds V. Zdimal *et al.*) 481-487 (International Society for Photogrammetry and Remote Sensing).

71 Felikson, D. *et al.* Comparison of Elevation Change Detection Methods from ICESat Altimetry over the Greenland Ice Sheet. *IEEE Trans Geosci Remote Sens* **55**, 5494-5505, doi:10.1109/TGRS.2017.2709303 (2017).

72 Helm, V., Humbert, A. & Miller, H. Elevation and elevation change of Greenland and Antarctica derived from CryoSat-2. *Cryosphere* **8**, 1539-1559, doi:10.5194/tc-8-1539-2014 (2014).

73 Ewert, H. *et al.* Precise analysis of ICESat altimetry data and assessment of the hydrostatic equilibrium for subglacial Lake Vostok, East Antarctica. *Geophys. J. Int.* **191**, 557-568, doi:10.1111/j.1365-246X.2012.05649.x (2012).

74 McMillan, M. *et al.* Increased ice losses from Antarctica detected by CryoSat-2. *Geophys. Res. Lett.* **41**, 3899-3905, doi:10.1002/2014GL060111 (2014).

75 Zwally, H. J. *et al.* Mass gains of the Antarctic ice sheet exceed losses. *J. Glaciol.* **61**, 1019-1036, doi:10.3189/2015JoG15J071 (2015).

76 Gunter, B. C. *et al.* Empirical estimation of present-day Antarctic glacial isostatic adjustment and ice mass change. *Cryosphere* **8**, 743-760, doi:10.5194/tc-8-743-2014 (2014).

77 Scambos, T. & Shuman, C. Comment on 'mass gains of the Antarctic ice sheet exceed losses' by H. J. Zwally and others. *J. Glaciol.* **62**, 599-603, doi:10.1017/jog.2016.59 (2016).

78 Zwally, H. J. *et al.* Response to Comment by T. SCAMBOS and C. SHUMAN (2016) on 'Mass gains of the Antarctic ice sheet exceed losses' by H. J. Zwally and others (2015). *J. Glaciol.* **62**, 990-992, doi:10.1017/jog.2016.91 (2016).

79 Richter, A. *et al.* Height changes over subglacial Lake Vostok, East Antarctica: Insights from GNSS observations. *J. Geophys. Res. F Earth Surf.* **119**, 2460-2480, doi:10.1002/2014JF003228 (2014).

80 Rignot, E., Velicogna, I., Van Den Broeke, M. R., Monaghan, A. & Lenaerts, J. Acceleration of the contribution of the Greenland and Antarctic ice sheets to sea level rise. *Geophys. Res. Lett.* **38**, doi:10.1029/2011GL046583 (2011).

81 Stocker, T. F. *et al. Climate change 2013 the physical science basis: Working Group I contribution to the fifth assessment report of the intergovernmental panel on climate change*. Vol. 9781107057999 (Cambridge University Press, 2013).

82 Bouman, J. *et al.* Antarctic outlet glacier mass change resolved at basin scale from satellite gravity gradiometry. *Geophys. Res. Lett.* **41**, 5919-5926, doi:10.1002/2014GL060637 (2014).

83 Konrad, H. *et al.* Uneven onset and pace of ice-dynamical imbalance in the Amundsen Sea Embayment, West Antarctica. *Geophys. Res. Lett.* **44**, 910-918, doi:10.1002/2016GL070733 (2017).

84 Gardner, A. S. *et al.* Increased West Antarctic and unchanged East Antarctic ice discharge over the last 7 years. *The Cryosphere* **12**, 521-547, doi:10.5194/tc-12-521-2018 (2018).

85 Hogg, A. E. *et al.* Increased ice flow in Western Palmer Land linked to ocean melting. *Geophys. Res. Lett.* **44**, 4159-4167, doi:10.1002/2016GL072110 (2017).

86 Pritchard, H. D., Arthern, R. J., Vaughan, D. G. & Edwards, L. A. Extensive dynamic thinning on the margins of the Greenland and Antarctic ice sheets. *Nature* **461**, 971-975, doi:10.1038/nature08471 (2009).

87 Li, X., Rignot, E., Morlighem, M., Mouginot, J. & Scheuchl, B. Grounding line retreat of Totten Glacier, East Antarctica, 1996 to 2013. *Geophys. Res. Lett.* **42**, 8049-8056, doi:10.1002/2015GL065701 (2015).

88 Lenaerts, J. T. M. *et al.* Recent snowfall anomalies in Dronning Maud Land, East Antarctica, in a historical and future climate perspective. *Geophys. Res. Lett.* **40**, 2684-2688, doi:10.1002/grl.50559 (2013).

Data Availability

The final mass balance datasets generated in this study are freely available at www.imbie.org.

Extended Data Legends

Extended Data Figure 1 | Ice sheet mass balance data sets included in this assessment. Some data sets did not encompass all three ice sheets.

Extended Data Figure 2 | Ice sheet drainage basins. Antarctic ice sheet drainage basins according to the definitions of Zwally [3] (top) and Rignot [2,20](bottom). Basins falling within the Antarctic Peninsula, West Antarctica, and East Antarctica are shown in green, pink and blue, respectively. For the Zwally definition, the Antarctic Peninsula, West Antarctica, and East Antarctica basins cover areas of 227 725 km^2, 1 748 200 km^2 and 9 909 800 km^2, respectively. For the Rignot definition, the Antarctic Peninsula, West Antarctica, and East Antarctica basins cover areas of 232 950 km^2, 2 039 525 km^2 and 9 620 225 km^2, respectively.

Extended Data Table 1 | Spatially-averaged Antarctic ice sheet surface mass balance. Estimates of the average surface mass balance (SMB) over the period 1980 to 2012 were derived from regional climate models (RCM) and global reanalyses (GCM). Data were evaluated using the Rignot drainage basins [2,20].

Extended Data Figure 3 | Temporal variations in Antarctic ice sheet surface mass balance. Time series of integrated surface mass balance in Antarctic ice sheet drainage regions (Rignot et al., 2011a, 2011b) from the MAR (blue) and RACMO2.3p (red) models.

Extended Data Figure 4 | Modeled glacial isostatic adjustment beneath the Antarctic Ice Sheet. Bedrock uplift rates in Antarctica averaged over the GIA model solutions submitted to the second IMBIE assessment (a), as well as their respective standard deviation (b).

Extended Data Table 2 | Glacial Isostatic Adjustment model details. Regional changes in mass associated with the glacial isostatic adjustment signal were determined from the model data ([†]) or calculated as an indicative rate using degrees 3-90 ([‡]).

[a] Main publication listed, in all cases additional supporting publications should be acknowledged in supp. info.

[b] Own model if not otherwise stated. Comma-separated values refer to properties of radially-varying (1D) Earth model: first value is lithosphere thickness (km), other values reflect mantle viscosity ($x10^{21}$ Pa s) for specific layers – see relevant publications for details

[c] Ice model covers at least Last Glacial Maximum to present, unless indicated

[d] GIA model details: SH=spherical harmonic (maximum degree indicated), FE=finite element, C=compressible, IC=incompressible, RF=rotational feedback, SG=self-gravitation, OL=ocean loading, 'x' = feature not included, UQ=uncertainty quantified

[e] RSL = relative sea-level data; GPS rates all corrected for elastic response to contemporary ice mass change

[f] Different to ICE-6G_C in Antarctica, due to use of BEDMAP2 [1] topography in that region

[g] Model relates to GIA in the northern Antarctic Peninsula only

[h] Model relates to GIA in the Amundsen Sea Embayment only

[i] 25

[j] 89

[k] 90

Extended Data Figure 5 | Individual rates of ice sheet mass balance. Mass balance estimates were determined from satellite altimetry (left), gravimetry (centre), and the input-output method (right) in the Antarctic Peninsula (top), East Antarctica (middle) and West Antarctica (bottom). The

ensemble average is shown as a dashed black line, with the estimates one sigma uncertainty as light grey shading. Also shown is the standard error of the mean solutions, per epoch (dary grey).

Extended Data Table 3 | Features of mass balance data sets included in this study. Details shown include their maximum span and ranges of temporal sampling, amplitude, estimated error, and standard deviation at each epoch.

Extended Data Table 4 | Aggregated estimates of ice sheet mass balance determined from satellite altimetry, gravimetry, and input-output method. In this comparison, the data were averaged over the period 2003 to 2010. Also shown is the arithmetic mean of each individual result for given regions, and the combined imbalance of the AIS, calculated as the sum of estimates from the constituent regions.

Extended data references

89 Pollard, D. & Deconto, R. M. Description of a hybrid ice sheet-shelf model, and application to Antarctica. *Geoscientific Model Dev.* **5**, 1273-1295, doi:10.5194/gmd-5-1273-2012 (2012).

90 Martinec, Z. Spectral-finite element approach to three-dimensional viscoelastic relaxation in a spherical earth. *Geophys. J. Int.* **142**, 117-141, doi:10.1046/j.1365-246X.2000.00138.x (2000).

a

Antarctic Peninsula

dM/dt (Gt/yr)

40 20 0 −20 −40 −60 −80 −100 −120 −140

3 3 3 3 3 3 3 3 3 3 4 20 22 22 22 22 21 17 17 17 17 16 14 2

1990 1995 2000 2005 2010 2015 2020

b

West Antarctica

dM/dt (Gt/yr)

100 50 0 −50 −100 −150 −200 −250 −300

4 4 4 4 4 4 4 4 4 4 5 21 23 23 23 23 22 18 18 18 18 17 15 2

1990 1995 2000 2005 2010 2015 2020

Year

c

East Antarctica

dM/dt (Gt/yr)

300 200 100 0 −100 −200 −300

4 4 4 4 4 4 4 4 4 4 5 21 23 23 23 23 22 18 18 18 18 17 15 2

1990 1995 2000 2005 2010 2015 2020

Year

Altimetry

Gravimetry

Input-Output Method

All

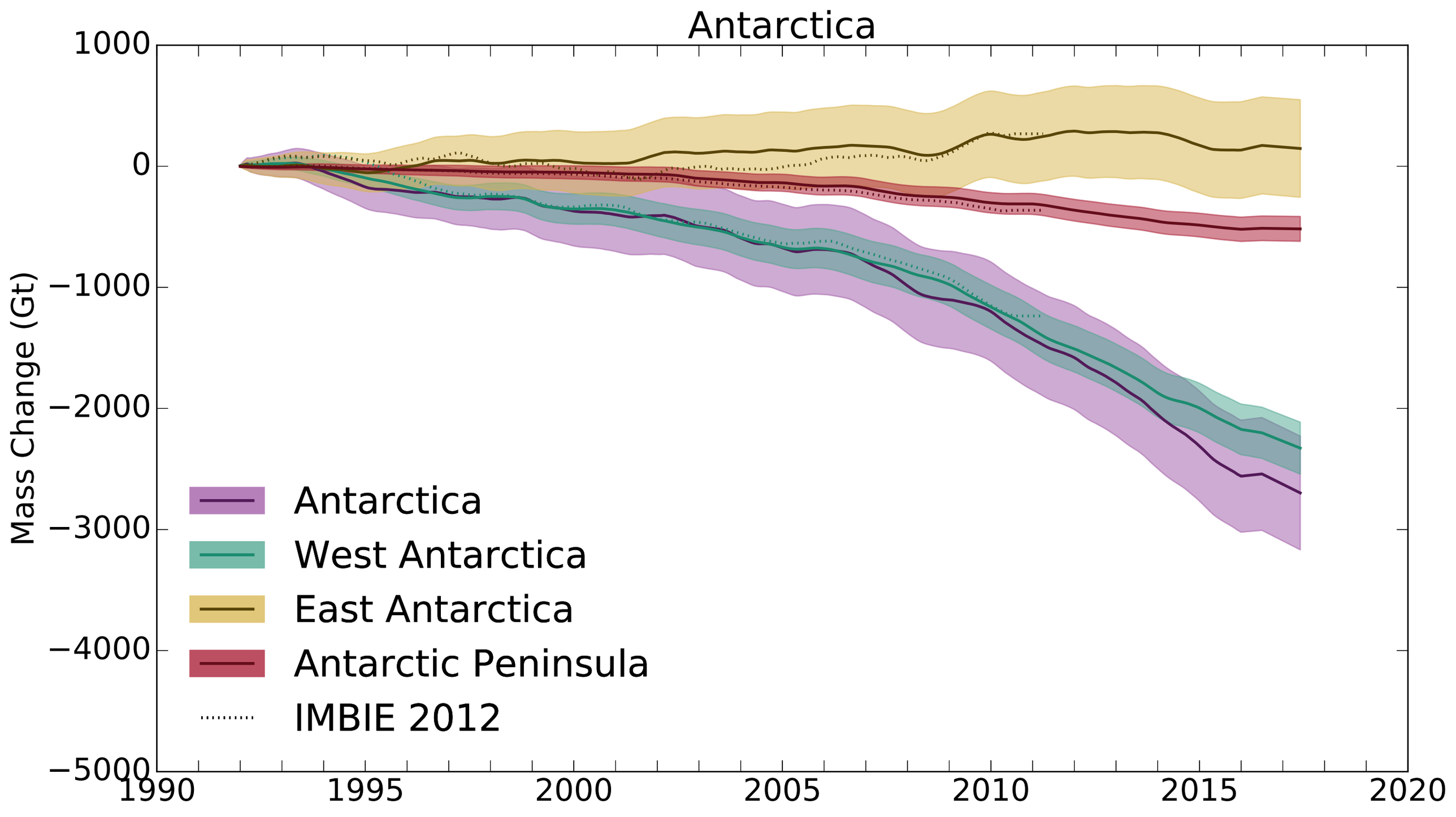
Antarctica
1000
0
−1000
−2000
−3000
−4000
−5000
Mass Change (Gt)
1990
1995
2000
2005
2010
2015
2020
Antarctica
West Antarctica
East Antarctica
Antarctic Peninsula
IMBIE 2012